J Mol Model (2014) 20:2482
DOI 10.1007/s00894-014-2482-3

ORIGINAL PAPER

An insight into the structures, stabilities, and bond character of B_nPt (n=1~6) clusters

Guangli Yang · Wenwen Cui · Xiaolei Zhu · Ruiying Yue

Received: 17 July 2014 / Accepted: 28 September 2014 / Published online: 15 October 2014

Abstract We perform a systematical investigation on the geometry, thermodynamic/kinetic stability, and bonding nature of low-lying isomers of B_nPt (n=1-6) at the CCSD(T)/[6-311+G(d)/LanL2DZ]//B3LYP/[6-311+G(d)/LanL2DZ] level. The most stable isomers of B_nPt (n=1-6) adopt planar or quasi-planar structure. B_nPt (n=2-5) clusters can be generated by capping a Pt atom on the B-B edge of pure boron clusters. However, For B_6Pt with non-planar structure, a single doped Pt atom significantly affects the shape of the host boron cluster. The dopant of the Pt atom can improve the stability of pure boron clusters. The valence molecular orbital (VMO), electron localization function (ELF), and Mayer bond order (MBO) are applied to gain insight into the bonding nature of B_nPt (n=2-6) isomers. The aromaticity for some isomers of B_nPt (n=2-6) is analyzed and discussed in terms of VMO, ELF, adaptive natural density partitioning (AdNDP), and nucleus-independent chemical shift (NICS) analyses. Results obtained from the energy and cluster decomposition analyses demonstrate that B_2Pt and B_4Pt exhibits as highly stable. Importantly, some isomers of B_nPt (n=2-5) are stable both thermodynamically and kinetically, which are observable in future experiment.

Keywords Aromaticity · Boron platinum cluster · Density functional theory · Potential energy surface · Stability

Electronic supplementary material The online version of this article (doi:10.1007/s00894-014-2482-3) contains supplementary material, which is available to authorized users.

G. Yang · W. Cui · X. Zhu (✉) · R. Yue
State Key Laboratory of Materials-Oriented Chemical Engineering, College of Chemistry and Chemical Engineering, Nanjing University of Technology, Nanjing 210009, China
e-mail: xlzhu@njtech.edu.cn

Introduction

It is well known that clusters have been considered a bridge between atoms (or molecules) and bulk, so the studies on clusters are very important for nanotechnological applications in the future. Because their unique physical and chemical properties such as structural, electronic, thermodynamic, and kinetic properties are not well understood, they are still the objects of intense research [1–5]. The *ab initio* methods and the density functional theory (DFT) [6, 7] have been regarded as powerful tools for predicting structures and properties of clusters, which can speed up experimental studies.

Recently, B_n clusters have been the topics of many experimental and theoretical studies because of the practical applications of boron and its chemical compound in the aerospace industry, electronic devices, and superconduction [8–10]. Very recently, much attention has been devoted to the investigations of the metal-doped boron clusters for their theoretical and practical values in many fields. For example, Chaudhari et al. used the B3LYP/LANL2DZ and B3LYP/SDD methods to analyze the lowest spin state, electron affinities, ionization potentials, and binding energies for X-B (X=La, Hf, Ta, W, Re, Os, Ir, Pt, Au, Hg), respectively [11]. The electronic structures of Ag, Au, and Cu doped-boron clusters [12–15] have been studied based on different theoretical methods. For Zr-doped boron clusters, Wang and coworkers [16] have found that dopant of the Zr atom can improve the stability of the pure boron clusters and the magic numbers of stability are 3, 7, 10 for the ZrB_n (n=1-12) clusters. Wu [17] reported that the most stable isomers of ScB_n(n=1-12) have planar or quasi-planar structure when n≤6, while from n≥7, the ground state isomers favor nest–like structure. For the stability of the ScB_n(n=1-12) clusters, the magic numbers are n=3, 7, 8, 9, and 11. Furthermore, the geometries, stabilities, electronic properties, and magnetism of FeB_n(n=1-10) clusters were systematically studied by DFT [18] method, and it is favorable

that the Fe atom locates at the surface, not at the center of the cluster. Each of some transition-metal-doped boron clusters [19–24] consists of a peripheral ring and one planar hypercoordinated metal atom. Many structures of optimized FeB_8, CoB_8, and FeB_9 [24] neutral and charged clusters have local D_{8h} and D_{9h} minima, but they are not the most stable isomers. Their aromaticities were discussed based on NICS at B3LYP/6-311G* and GIAO/B3LYP/6-311G* levels. Yan et al. [25] studied the stabilities of MB_n (M=Y, Zr, Nb, Mo, Tc, Ru, $n \leq 8$) clusters. They found YB_7, ZrB_7, NbB_6, MoB_6, TcB_6, RuB_6 clusters possess relatively higher stabilities. B_{32} and metal-poly-boron isomers MB_{32} [26] (M=Li, Na, K, Be, Ca) are optimized using the B3LYP/6-31G(d) theoretical level followed by vibrational frequency and NBO analyses. Wang et al. [27] investigate the feasibility of bare and metal-coated boron buckyballs B_{80} with M=Li, Na, K, Be, Mg, Ca, Sc, Ti, and V for hydrogen storage.

Despite the existing studies of metal-doped boron clusters [11–28] as mentioned above, there is a lack of systematic reporting on kinetic stability of metal-doped boron clusters, which can reveal the possibilities of detecting them in future experiment. On the other hand, since the potential energy surface becomes very complicated as the total number of cluster atoms increases, to reveal the kinetic stability of metal-doped boron clusters is important and challenging. In the current work, first, we comprehensively located the geometrical structures of low-lying isomers for B_nPt (n=1-6) at the CCSD(T)/[6-311+G(d)/LanL2DZ]//B3LYP/[6-311+G(d)/LanL2DZ] level. Then, we focused on the analyses on thermodynamic/kinetic stability of the low-lying isomers of B_nPt (n=1-6) clusters. Finally, the bonding character of B_nPt (n=1-6) isomers is examined and revealed. This work will provide a systematical insight into the structure and stability of B_nPt (n=1-6) clusters for future experimental studies.

Computational details

In the current work, in order to examine and investigate the geometrical structures and potential energy surfaces (PESs) of B_nPt (n=1-6) isomers, both randomized algorithms and exhaustive search method [29, 30] are applied to located possible isomers of B_nPt (n=1-6) clusters with two different spin multiplicities (doublet and quartet states for BPt, B_3Pt, and B_5Pt clusters, and singlet and triplet states for B_2Pt, B_4Pt, and B_6Pt). The LanL2dz [31–33] pseudopotential is used for Pt atom, and 6-311+G(d) [34, 35] for boron atom. The low-lying isomers are optimized at the B3LYP/[6-311+G(d)/LanL2DZ] level [36–40]. The vibrational frequency analysis is carried out at the same level to examine whether the optimized structures are local minima or transition states. On the other hand, in order to analyze and examine the isomerization processes of the low-lying isomers of B_nPt (n=2-5), transition states are searched at the B3LYP/[6-311+G(d)/LanL2DZ] level. The energy calibration for optimized geometries of isomers and transition states is performed at the CCSD(T)/[6-311+G(d)/LanL2DZ] level to acquire more accurate energies. Finally, for the transition states, the intrinsic reaction coordinate (IRC) computations are carried out at the B3LYP/[6-311+G(d)/LanL2DZ] level to examine whether they connect the related isomers. Additionally, in order to examine the reliability of calculated results at the CCSD/[6-311+G(d)/LanL2DZ]//B3LYP/[6-311+G(d)/LanL2DZ] level, we also optimized all possible planar isomers at the MP2/[aug-cc-pVDZ/anL2DZ] level and calibrated their energies at the CCSD/[aug-cc-pVDZ/LanL2DZ]//MP2/[aug-cc-pVDZ/LanL2DZ] level. All calculations are carried out in the Gaussian 09 program package [41].

Results and discussion

Figures 1 and 2 show the optimized geometries of B_nPt (n=1-6) isomers and transition states (BPt, B_3Pt, and B_5Pt clusters with doublet and quartet states, and B_2Pt and B_4Pt with singlet and triplet states) respectively. The relative energies of the lower-energy isomers of B_nPt (n=1-6) and transition states are listed in Tables 1 and 2, respectively, at the B3LYP/[6-311+G(d)/LanL2DZ] and CCSD/[6-311+G(d)/LanL2DZ] levels for comparison. Briefly, alphabetical orders (such as a, b, c…) are used to represent the number of boron atoms and arab numbers are arranged in the order of energy increasing at the CCSD(T)/[6-311+G(d)/LanL2DZ]//B3LYP/[6-311+G(d)/LanL2DZ] level (For simplicity, it is marked as CCSD/B3LYP level hereunder).

Geometry and thermodynamic stability

For all possible isomers of BPt, two BPt isomers are **a1** ($C_{\infty v}$, $^2\sum$) and **a2** ($C_{\infty v}$, $^4\sum$) with doublet and quartet states, respectively, as shown in Fig. 1. The ground state of BPt is a linear isomer with B-Pt bond length of 1.781 Å, which is close to previous theoretical result [11] (1.809 Å at the B3LYP/LanL2DZ level). Isomer **a2** is 65.7 and 72.5 kcal·mol^{-1} higher than the ground state **a1** at the B3LYP and CCSD levels, respectively.

As shown in Fig. 1, the lowest-energy isomer of B_2Pt, **b1** (C_{2v}, $^1A_1$), has similar structure to those of B_3 [42] and Pt_3 [43] with an isosceles triangle. The B-Pt and B-B bond lengths in **b1** are 1.574 Å and 1.184 Å, respectively. The triplet isomer **b2** (C_{2v},$^3A_2$) with analogous structure to **b1** is 28.7 and 36.2 kcal·mol^{-1} higher than **b1** in energy at the B3LYP and CCSD levels, respectively. Isomers **b3** ($C_{\infty v}$, $^1\sum$) **and b4**($C_{\infty v}$, $^3\sum$) with the relative energies (37.5 and 43.8 kcal·mol^{-1} at the CCSD level) have B-B-Pt linear structure. To examine the reliability of calculated results at the

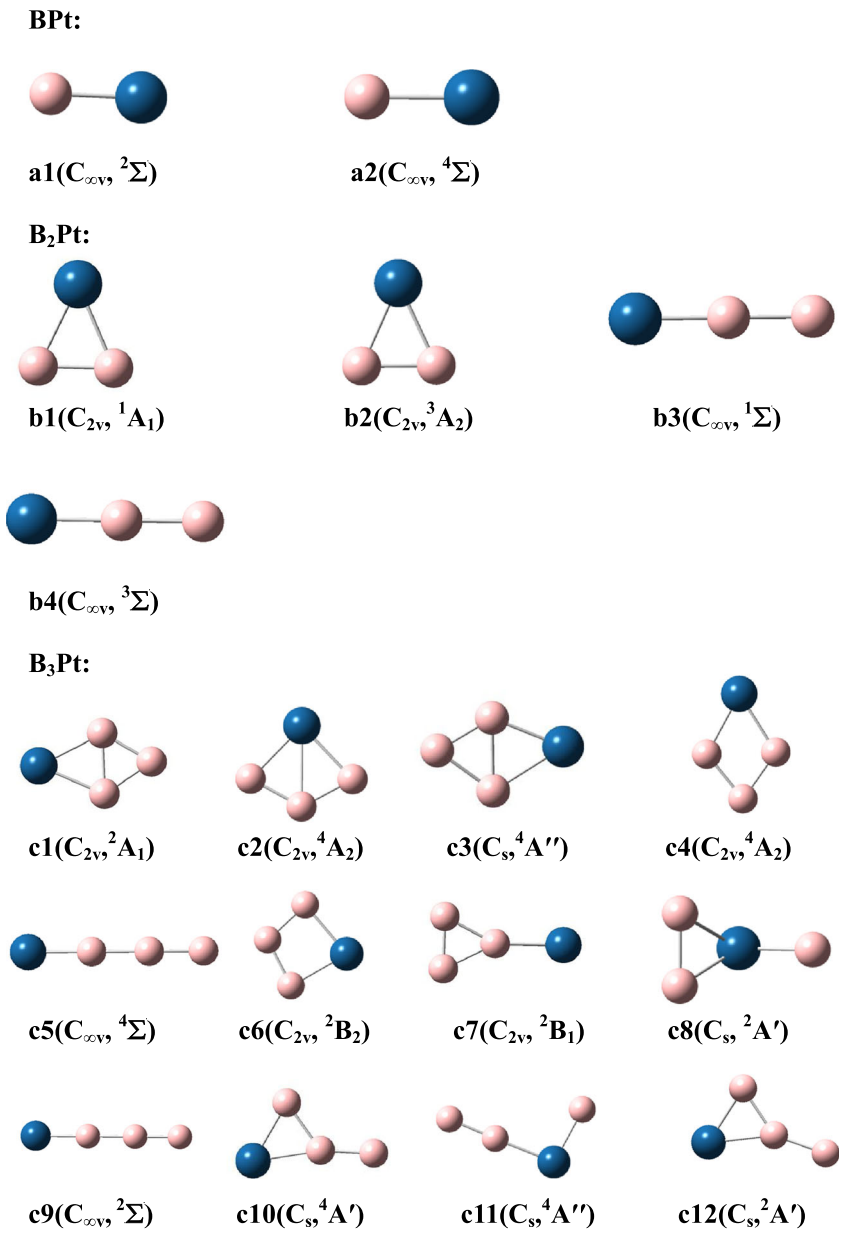

Fig. 1 The optimized geometries of lower-energy isomers for B_nPt (n=1-6) at the B3LYP/[6-311+G(d)/LanL2DZ] level. Point groups and electronic states are represented in parentheses. The blue and pink balls account for platinum and boron atoms, respectively

CCSD/[6-311+G(d)/LanL2DZ]//B3LYP/[6-311+G(d)/LanL2DZ] level, we also optimized all possible planar isomers at the MP2/[aug-cc-pVDZ/LanL2DZ] level and calibrate their energies at the CCSD/[aug-cc-pVDZ/LanL2DZ]//MP2/[aug-cc-pVDZ/ LanL2DZ] level. Figure SI-1 shows the structures of isomers for B_2Pt at the B3LYP/[6-311+G(d)/LanL2DZ] and MP2/[aug-cc-pVDZ/anL2DZ] levels, respectively. Obviously, the geometrical patterns, bond lengths, and bond angles for isomers of B_2Pt are similar at the B3LYP/[6-311+G(d)/LanL2DZ] and MP2/[aug-cc-pVDZ/anL2DZ] levels.

In the case of B_3Pt, the geometries of 14 low-lying isomers (**c1~c14**) of B_3Pt are represented in Fig. 1. The lowest energy structure of B_3Pt is **c1(C_{2v},$^2A_1$)** with B-Pt and B-B bond lengths of 1.184 Å and 1.512 Å, respectively. Isomer **c1** can be generated by substituting the three Pt atoms of Pt_4 cluster with three B atoms [43] and is similar to the lowest-energy isomers of AlB_3 [44], SrB_3 [16], and ScB_3 [17] or the fourth low-energy isomer of B_3Fe [18] in the structure. **c1** has B-Pt-B and B-B-B isosceles triangles. The structure of **c2(C_{2v},$^4A_2$)** with two symmetrical B-Pt-B triangles is 17.4 and 18.8 kcal·mol^{-1} higher than the ground state **c1** at the B3LYP and CCSD levels, respectively. **c2** and **c1** possess different inner bonds (B-Pt bond in **c2** and B-B bond in **c1**). The quartet isomer **c3(C_s,$^4A''$)** has similar geometry to **c1** with 22.7 kcal·mol^{-1} higher than the ground state **c1** in energy

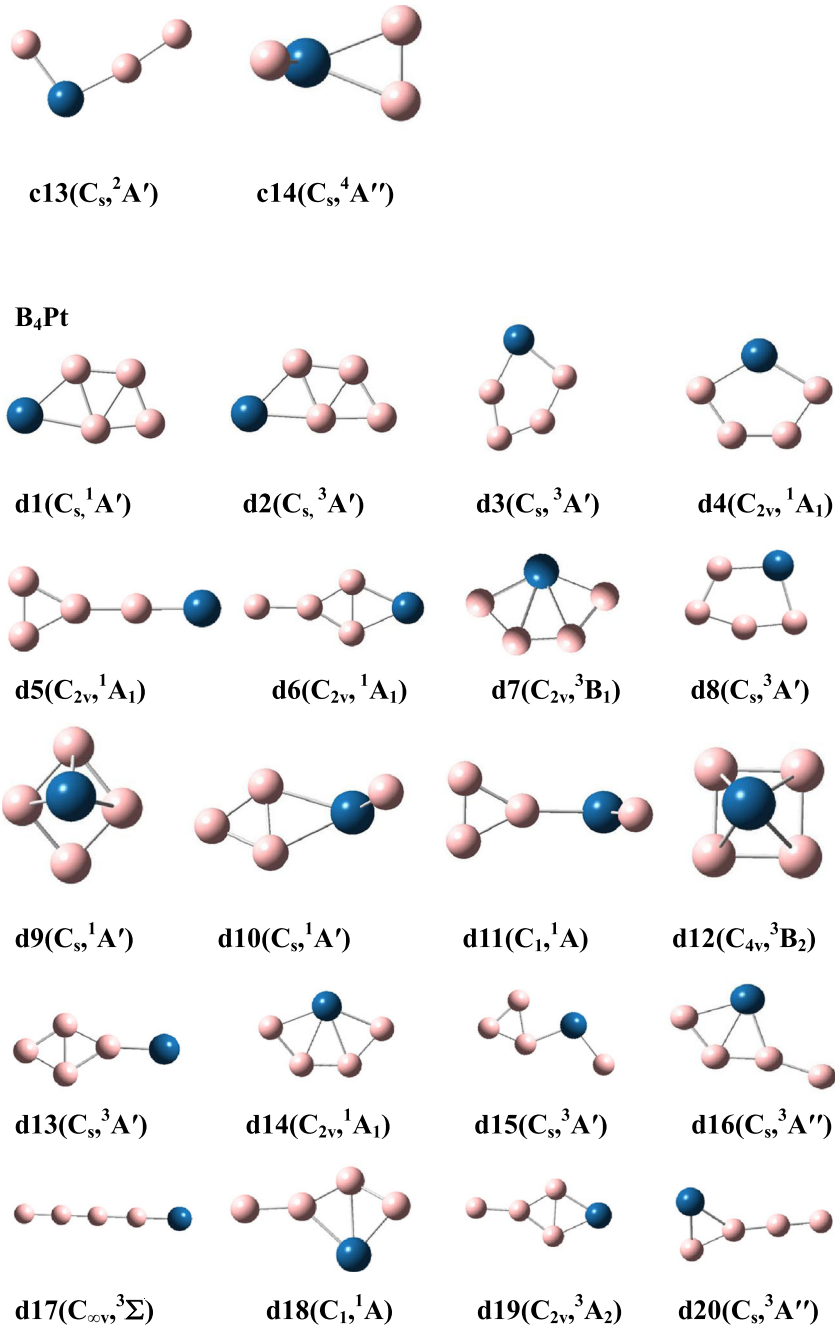

Fig. 1 (continued)

at the CCSD/[6-311+G(d)/LanL2DZ] level. **c4 (C_{2v},$^4A_2$)** has planar rhombic geometry with Pt-B and B-B bond lengths of 1.934 and 1.613 Å, respectively, and the B-Pt-B angle of 60.1°. The lowest energy state of B_4 [42] and B_3C [45] is similar to **c4** in structure. The Pt-B-B-B linear isomers **c5** ($C_{\infty v}$, $^4\Sigma$) and **c9** ($C_{\infty v}$, $^2\Sigma$) are 28.6 and 39.6 kcal·mol^{-1} higher in energy than **c1** at the CCSD level, respectively. **c6** (C_{2v}, $^2B_2$) possesses a similar structure to **c4**. Isomers **c7**, **c10**, and **c12** have similar geometries with one three-membered ring and one exocyclic chain. The quartet **c11** is similar to doublet **c13** with nonlinear structure. The spatial structure **c8** (spin multiplicity=2) and **c14** (spin multiplicity=4) with one boron atom locating above the B-B-Pt three-ring plane are higher in energy than **c1** by 49.4 and 58.6 kcal·mol^{-1}, respectively.

As for B_4Pt, as shown in Fig. 1, **d1(C_s,$^1A'$)** is the most stable isomer of B_4Pt with one BPtB three-membered ring and two BBB three-membered rings, which can be viewed as attaching one Pt atom to B_4 [42] with an inner B-B bond. It is interesting to note that all MB_4 (M=Sc, Al, and C) [17, 44,

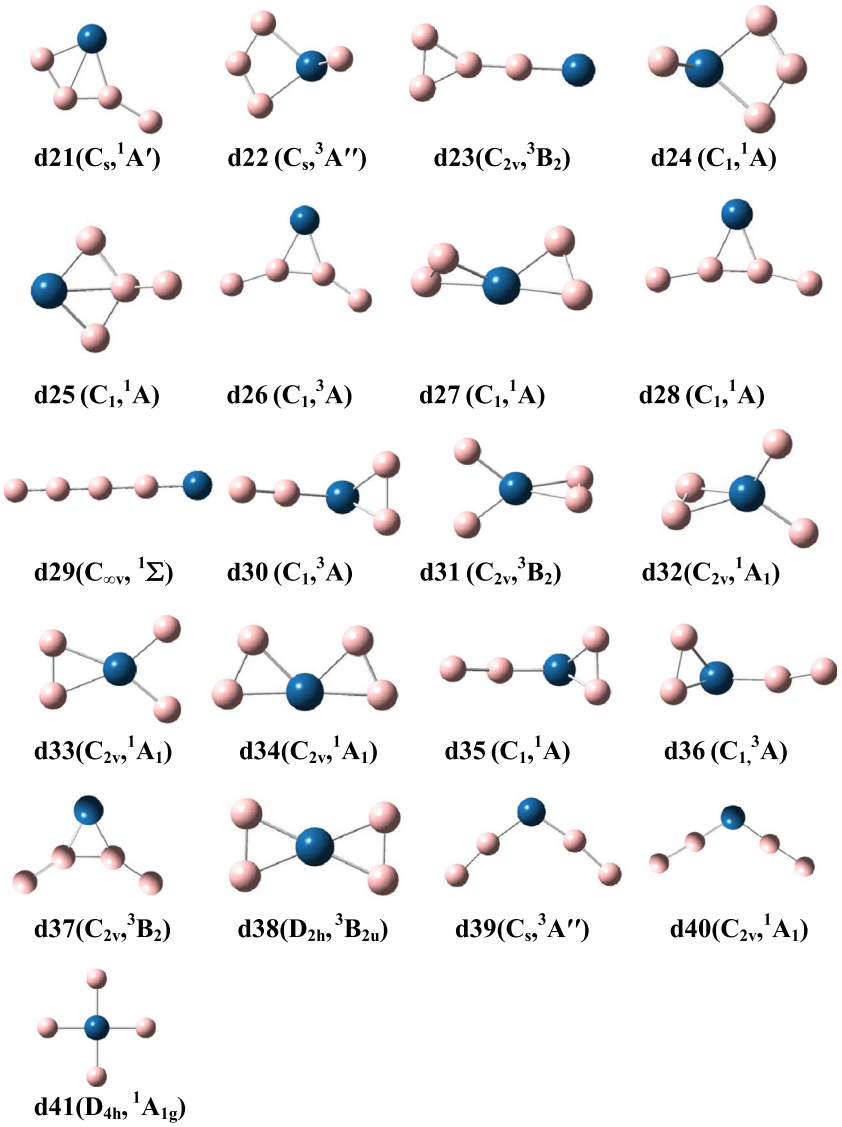

Fig. 1 (continued)

45] isomers prefer the structure of **d1. d2(C_s, ^{3}A′)** has a similar structure to **d1**. Both **d3(C_s, ^{3}A′)** and **d4(C_{2v},$^1A_1$)** include five-membered monocyclic structure. It is noted that the relative energies of singlet **d4** and **d5** are the 37.4 and 37.4 kcal·mol^{-1} at the CCSD level, respectively, suggesting that they are almost isoenergetic. **d6**, **d13**, **d16**, **d19**, and **d21** have one four-membered ring and one exocyclic chain. Isomers **d7(C_{2v},$^3B_1$)** and **d8(C_s,^{3}A′)** contain a five-membered ring, while **d7** has a tetra-coordinated Pt atom. The pyramid isomers **d9** and **d12** with different spin multiplicities include one Pt atom located at the top of B-B-B-B plane. The non–planar structures of **d10**, **d11**, **d22**, **d24**, and **d25** can be ascribed to exocyclic chains. The triplet **d14** has similar structure to singlet **d7** with one tetra-coordinated Pt atom. Each of **d15**, **d20**, and **d23** has one three-membered ring and one exocyclic chain. The **d17($C_{\infty v}$,$^3\sum$)** with BBBBPt linear structure is 69.2 kcal·mol^{-1} higher than the most stable isomer (**d1**) at the CCSD/[6-311+G(d)/LanL2DZ] level. Isomers **d29-d41** have higher relative energy than other isomers of B_4Pt (>100 kcal·mol^{-1} at the CCSD level) as shown in Table 1.

The geometries of 33 low-lying isomers of B_5Pt are presented in Fig. 1. The most stable isomer of B_5Pt, **e1(C_s,^{2}A′),** can be obtained by attaching one Pt atom to B_5 [42] with the B-B inner bond. The second lower-energy **e2(C_s,^{2}A′)** with one BPtB three-membered ring and three BBB three-membered rings is 7.2 kcal·mol^{-1} higher than **e1**. The doublet **e3** with a six-membered ring is 12.4 kcal·mol^{-1} higher than the ground state at the CCSD level. The **e4** has a pyramid structure similar to ScB_5 [17] and MoB_5 [25]. **e5**, **e7**, **e8**, **e12**, **e13**, **e15**, **e16**, **e18**, **e21**, and **e22**, have ring structures, in which **e8**, **e12**, **e15**, **e18**, **e21**, and **e22** possess quasi-planar structure. The isomer **e6 (C_s,^{2}A″)** is distorted to non–planar

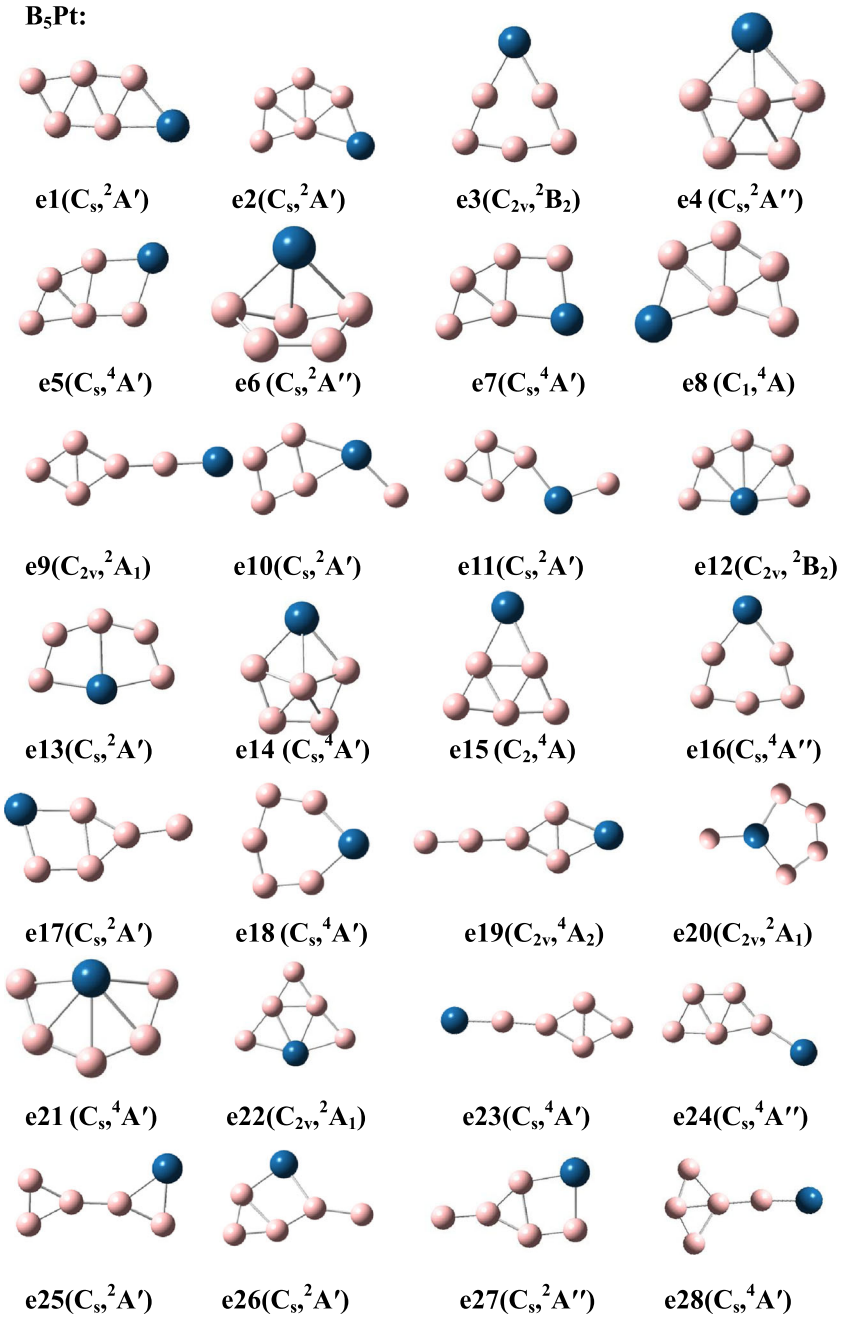

Fig. 1 (continued)

structure. The quartet **e14** has the pyramid structure. The structure of **e25** includes two triangles, the remaining isomers have one ring and one exocyclic chain except **e33. e33** with a linear PtBBBBB structure of 67.0 and 79.7 kcal·mol^{-1} higher than the lowest-energy isomer of B_5Pt at the B3LYP and CCSD levels, respectively.

With respect to B_6Pt, as shown in Fig. 1, the most stable isomer (**f1**) of B_6Pt adopts qusi-planar structure, which can be viewed as substituting a circumferential B atom of the most stable B_7 [42] with a Pt atom and has analogous structure to ScB_6 [17]. **f2** is 3.3 and 3.2 kcal·mol^{-1} higher than the lowest-energy isomer (**f1**) at the CCSD/[6-311+G(d)/LanL2DZ] and CCSD/[6-311++G(3df,2p)/LanL2DZ] levels, respectively, suggesting that **f1** and **f2** are almost isoenergetic. Isomers **f2**, **f3**, **f5**, and **f18** have quasi-planar structure. **f4(Cs,^{3}A″)** possesses one BPtB three-membered ring and four BBB three-membered rings, which can be obtained by capping a boron atom on B-B edge at the right corner of **e1** and is similar to the most stable planar isomer of B_6Fe [18]. **f6** contains four BBB three-membered rings with 1.9 kcal·mol^{-1} higher than **f4** at

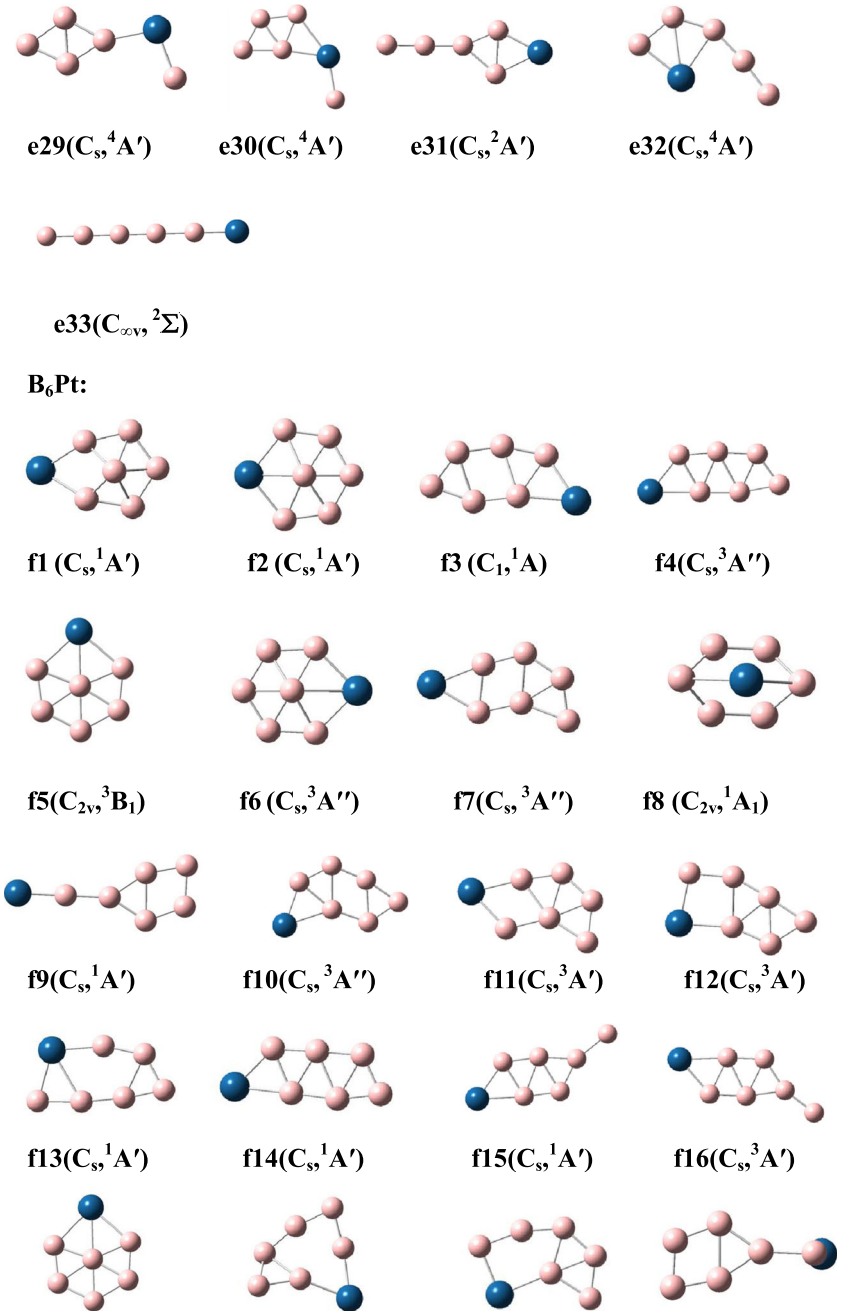

Fig. 1 (continued)

the CCSD level. Clearly, **f4** and **f6** with cyclic structure are almost isoenergetic. Isomers **f7**, **f10**, **f11**, **f12**, **f13**, **f19**, and **f27** adopt a similar seven-membered ring structure and different inner bonds. Isomer **f8** with C_{2v} symmetry possesses a platinum atom locating above the plane six-membered boron ring. For planar isomers **f9**, **f15**, **f16**, **f23**, **f25** and **f40**, they include one ring and one exocyclic chain. **f14 (C_s,^{1}A′)** has a similar geometry to **f4** with relative energy 28.3 kcal·mol^{-1}. In addition, **f17** is similar to **f5** in structure. The remaining isomers have three-dimensional framework.

It is interesting to note from Fig. 1 that the lowest-energy geometries of B_nPt (n=2-5) clusters exhibit planar polycyclic geometry, in which the numbers of triangles increase with increasing n. BPt has linear structure while the ground state isomer of B_6Pt adopts quasi–planar structure. Moreover, the lowest-energy isomers of B_nPt (n=2-5) can be generating by capping a Pt atom on B-B edge of B_n (n=). Additionally, B_nPt (n=1-6) isomers with lower spin states are lower in energy than corresponding isomers with higher spin states. The energy differences between lowest-energy isomer and second

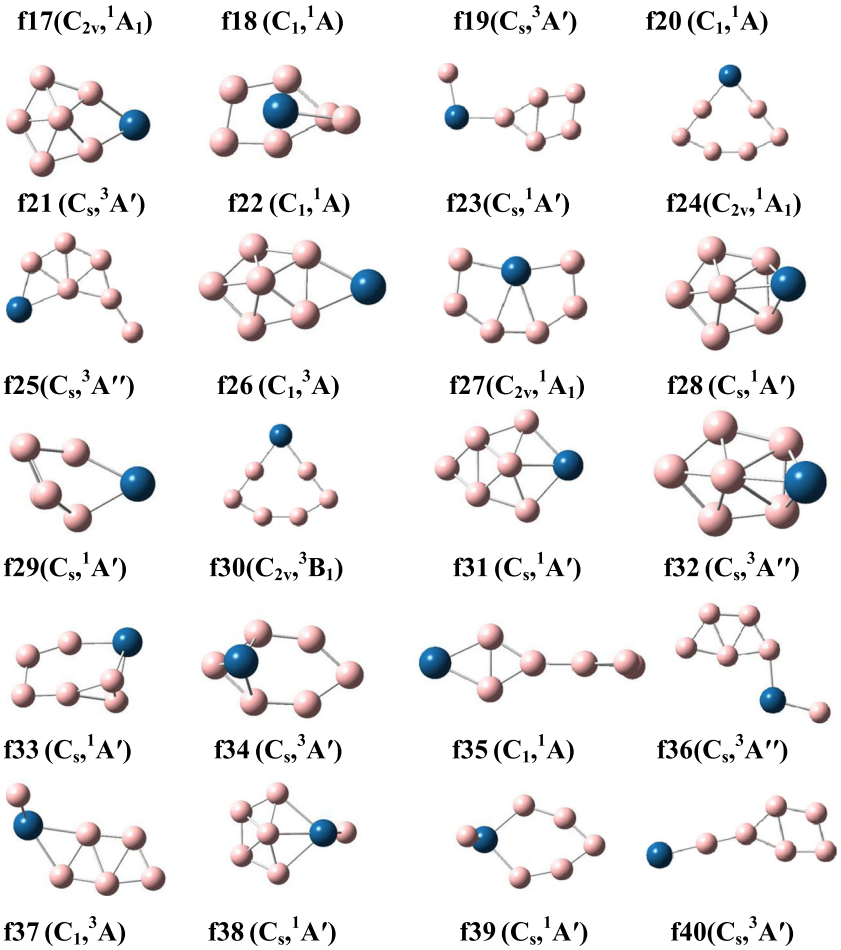

Fig. 1 (continued)

lower-energy isomer for B_nPt (n=1-4) are relatively larger as shown in Table 1.

In order to analyze and examine the relative stability [46] of B_nPt (n=1-6) clusters, the binding energy per atom (BE), incremental binding energy (IBE), and second order energy difference (Δ^2E) are analyzed. As shown in Fig. 3, the binding energies per atom of the B_nPt clusters are significantly larger than those of the pure B_n clusters, which reveal that the doped Pt atom significantly improves the stability of the B_n clusters and in agreement with the results from B_nZr [16] and B_nAl [44]. Figures 4(a)-(c) demonstrate that B_2Pt and B_4Pt have relatively larger BE, IBE, and Δ^2E values, suggesting their high stability. The HOMO–LUMO gaps, adiabatic ionization energy (AIP), and adiabatic electron affinity (AEA) for B_nPt clusters are shown in Fig. 4(d) and (e), respectively. Clearly, B_2Pt and B_4Pt possess relatively larger HOMO–LUMO gaps and AIP values, and smaller AEA values, which confirms that B_2Pt and B_4Pt exhibit higher stability. For further revealing the stability of B_nPt clusters, we analyze all the possible decompositions of the lowest energy planar structure at the B3LYP and CCSD levels. The relative decomposition energies of those structures are summarized in Table 3. The most likely decomposition reactions can be expressed by:

$$B_nPt \rightarrow B_{n-1}Pt + B$$

$$B_nPt \rightarrow B_{n-1} + BPt$$

As shown in Table 3, for decomposition reactions $B_nPt \rightarrow B_{n-1}Pt+B$ and $B_nPt \rightarrow B_{n-1}+BPt$, B_4Pt has the largest decomposition energies (122.6 and 122.7 kcal·mol^{-1}), suggesting that B_4Pt is highly stable. The results obtained from Fig. 4 and Table 3 reveal that B_2Pt and B_4Pt have high stability and may be magic clusters.

Isomerization and kinetic stability

Based on the planar isomers of B_nPt (n=2-5), the 52 transition states (one for triplet B_2Pt, four for doublet B_3Pt, five for quartet B_3Pt, seven for singlet B_4Pt, seven for triplet B_4Pt, 15 for doublet B_5Pt, and 13 for quartet B_5Pt) of B_nPt (n=2-5) at the B3LYP level are located and represented in Fig. 2. Here,

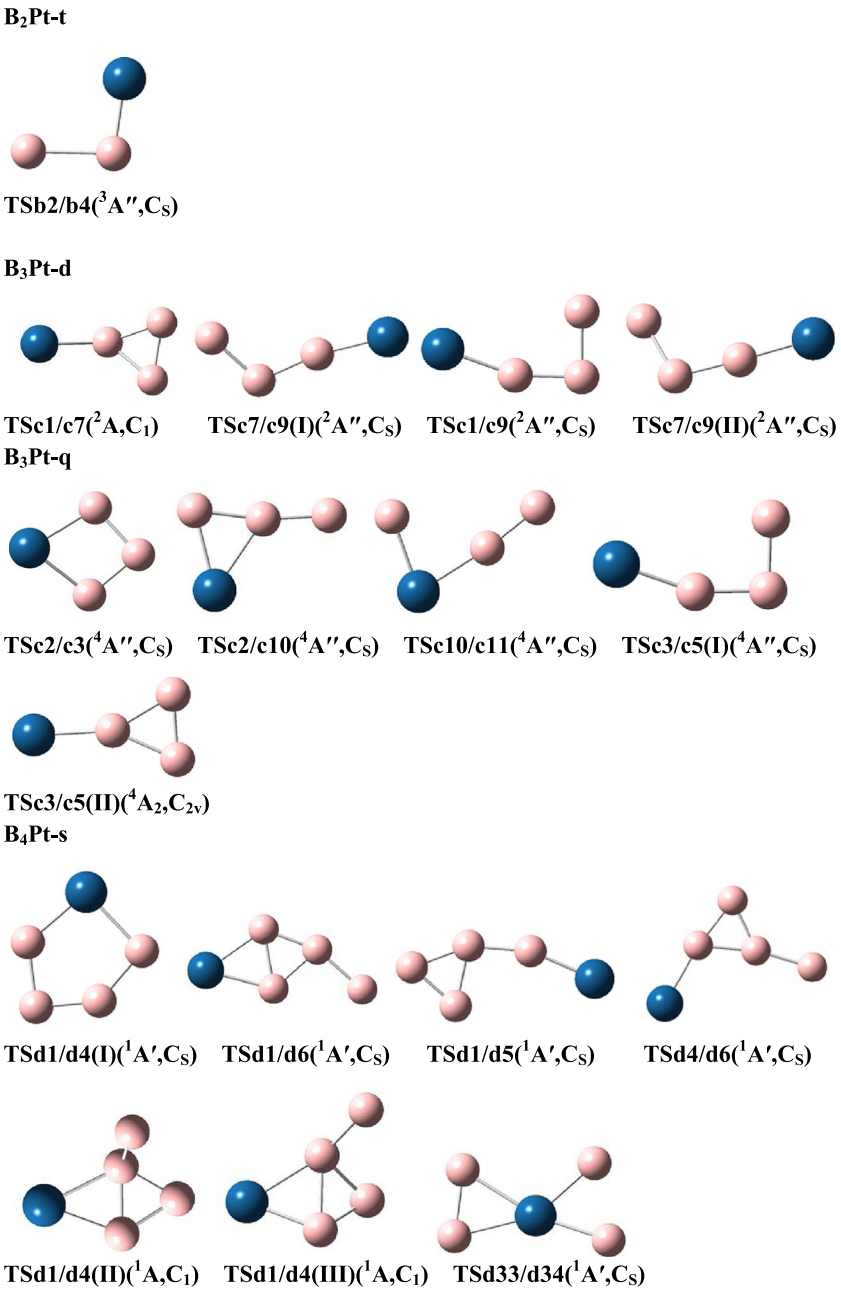

Fig. 2 The optimized structures of transition states for B_nPt (n=1-6) at the B3LYP/[6-311+G(d)/LanL2DZ] level. Point groups and electronic states are represented in parentheses. The blue and pink balls account for platinum and boron atoms, respectively

the structure details of transition states are not discussed for simplicity. In order to investigate the kinetic stability of B_nPt (n=2-5) isomers, various isomerization processes are examined and explored. In current calculations, the dissociation transition states are not searched since the relative energies of all possible dissociation fragments are relatively higher compared to lowest-energy isomers (>86 kcal·mol^{-1}) at the CCSD/B3LYP level as displayed in Table SI-1. Thus, the smallest conversion energy barriers are applied to reveal the kinetic stability of isomers for B_nPt (n=2-5) clusters.

For triplet states of B_2Pt, only one transition state is located as shown in Fig. 2. The PES of singlet B_2Pt is simple, which is not displayed here. Isomers **b2** and **b4** are kinetically stable since their conversion barriers (**b2**→**b4**) and (**b4**→**b2**) are 57.4 and 49.8 kcal·mol^{-1} at the CCSD(T) level, respectively.

The potential energy surface (PES) of doublet B_3Pt at the CCSD(T)/B3LYP level is represented in Fig. 5. As shown in Fig. 5, isomers **c1** (35.9 kcal·mol^{-1} for **c1**→**c7**), **c2** (11.7 kcal·mol^{-1} for **c2**→**c3**), **c5** (19.0 kcal·mol^{-1} for **c5**→**c3**), **c9** (11.4 kcal·mol^{-1} for **c9**→**c7**), are highly kinetically

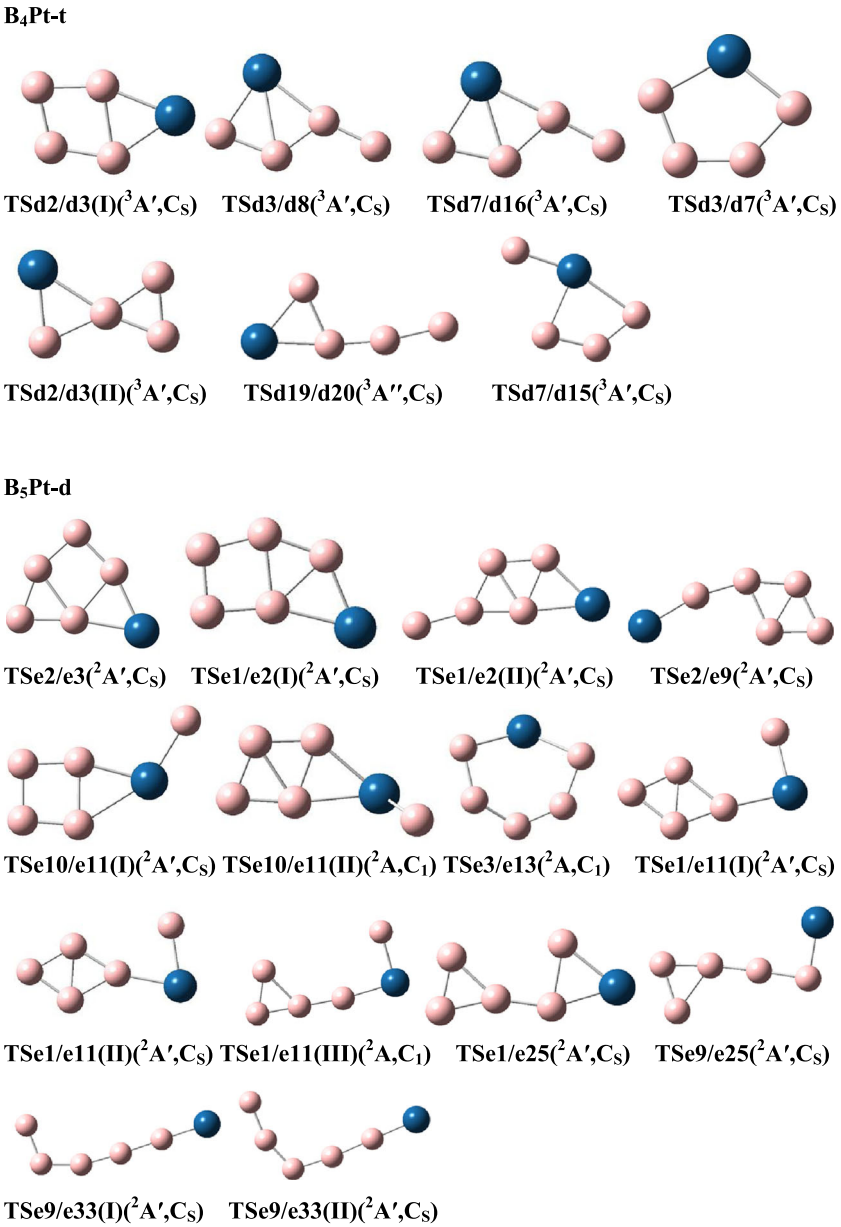

Fig. 2 (continued)

stable since their barrier energies are larger than 10 kcal·mol^{-1}. **c3**, **c7**, **c10**, and **c11** with conversion barriers of 9.4 (**c3→c2**), 1.0 (**c7→c1**), 2.3 (**c10→c2**), 0.8 (**c11→c10**) kcal·mol^{-1} are kinetically unstable. We do not obtain transition states about isomers **c4**, **c6**, **c12**, and **c13**. Owing to the three-dimensional structures of **c8** and **c14**, their transition states are not considered in the current work. It is interesting to find that some isomer pairs (**c3/c5** and **c7/c9**) have two isomerization channels. The most stable isomer **c1** can be transferred into **c7** (with a three-membered ring and one exocyclic chain) and **c9** (with a linear structure) through different isomerization channels. The conversion process (**c2→c3**) via TS**c2/c3** is accompanied by breaking an inner B-Pt bond and forming an inner B-B bond. During the conversion process (**c2→c10**) via TS**c2/c10,** the B-Pt bond is broken. **c10** and **c11** can be transformed into each other via TS**c10/c11**.

For singlet B_4Pt, the PES at the CCSD(T)/B3LYP level is displayed in Fig. 6. As represented in Fig. 6, the smallest conversation barriers of **d1** and **d5** are 47.1 (**d1→d4**) and 14.2 (**d5→d1**) kcal·mol^{-1}, respectively, resulting in the high kinetic stability of them. **d4**, **d6**, **d33**, and **d34** are kinetically unstable since their smallest isomerization barriers are less than 10 kcal·mol^{-1} (9.7 (**d4→d1**), 7.4 (**d6→d1**), 1.5 (**d33→d34**), and 1.0 (**d34→d33**) kcal·mol^{-1}, respectively). Additionally, there are not transition states located about **d14**, **d21**, and **d29**. The ground state (**d1**) of B_4Pt can be transformed into

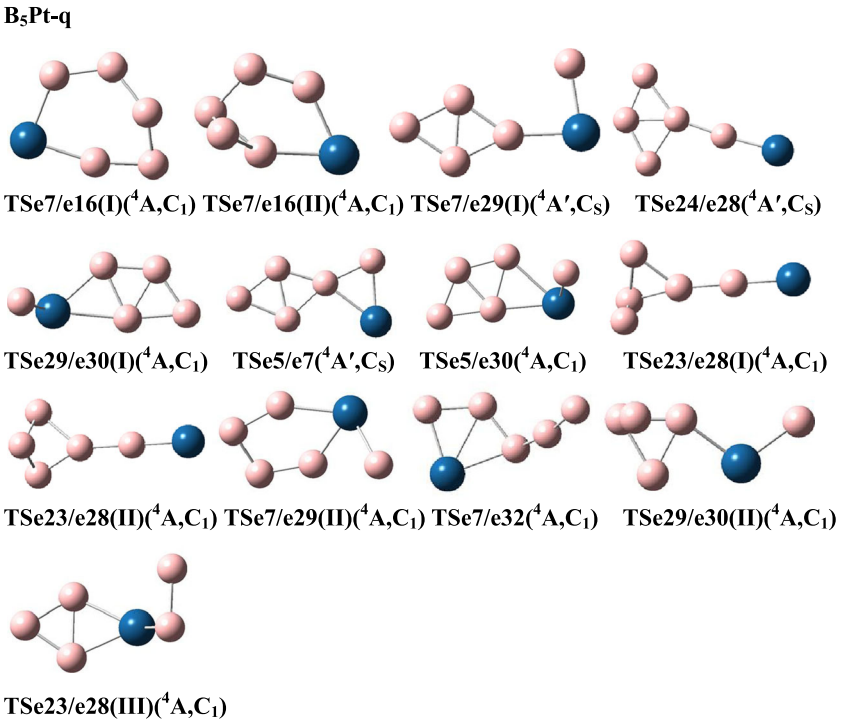

Fig. 2 (continued)

d4 through three direct isomerization channels. The structure of TS**d1/d4(I)** is similar to **d4** with the relative energy of 47.1 kcal·mol^{-1} at the CCSD(T) level as shown in Table 2. TS**d1/d4(II)** and TS**d1/d4(III)** have similar structures with a four-membered ring and one exocyclic chain. Moreover, **d1** (with one B-Pt-B triangle and two B-B-B triangles) can is transferred into **d5** (with one B-B-B triangle and one exocyclic chain) and **d6** (with one four-membered ring and one exocyclic chain) via two different isomerization channels, respectively, which include the breaking of B-Pt bond. Isomer **d4** with five-membered ring structure is difficult to convert into **d6** owing to the high conversion barrier of 29.6 kcal·mol^{-1} at the CCSD(T) level. It is due to the fact that the conversion is realized through the breaking of B-Pt bond and the forming of B-B bond. Clearly, B-Pt bond is significantly stronger than B-B bond. However, it is easier for **d33** to transfer into **d34** with a low conversion barrier of 1.5 kcal·mol^{-1}, which may be ascribed to that the structures of **d33** and TS**d33/34** are similar.

The PES of triplet B_4Pt is shown in Fig. 7. **d7** (**d7**→**d16** conversion), **d15** (**d15**→**d7** conversion), **d19** (**d19**→**d20** conversion), and **d20** (**d20**→**d19** conversion) are kinetically stable with corresponding isomerization barriers of 28.5, 23.1, 11.0, and 10.6 kcal·mol^{-1}, respectively. The lowest barriers of the remaining isomers (**d2**, **d3**, **d8**, and **d16**) are 6.9 (**d2**→**d3**), 2.1 (**d3**→**d2**), 3.2 (**d8**→**d3**), and 0.1 (**d16**→**d7**) kcal·mol^{-1}, leading to being kinetically unstable. The transition states about **d13**, **d17**, and **d23** are not located in this work. **d2/d3** converting into TS**d2/d3(I)** needs to break/form a B-B bond with conversation barrier of 6.9/2.1 kcal·mol^{-1}. TS**d2/d3(II)** with a butterfly-like structure is different from TS**d2/d3(I)**. Isomer **d3** can be transferred into TS**d3/d8**, which is accompanied by breaking B-B bond and forming B-Pt bond and another B-B bond. It is interesting to note that the conversion barrier (0.1 kcal·mol^{-1} for **d16**→**d7**) of **d16** is significantly smaller than that (28.5 kcal·mol^{-1} for **d7**→**d16**) of **d7,** which is possibly due to the similar structures of **d16** and TS**d7/d16**. Isomer **d7** can be transferred into three isomers **d3**, **d15**, and **d16** through different isomerization channels, respectively. **d19** (with four-membered ring and one exocyclic chain) needs to break one B-B bond to isomerize into **d20** (with one three-membered ring and one exocyclic chain) through TS**d19/d20**.

Figure 8 illustrates the PES of doublet B_5Pt at the CCSD/B3LYP level. Isomers **e1** (**e1**→**e2**), **e25** (**e25**→**e1**) and **e33** (**e33**→**e9**) with isomerization barriers of 15.8, 16.4, and 10.8 kcal·mol^{-1}, respectively, are stable kinetically while isomer **e2** (**e2**→**e3**), **e3** (**e3**→**e2**), **e9** (**e9**→**e2**), **e10** (**e10**→**e11**), **e11** (**e11**→**e10**), and **e13** (**e13**→**e3**) are unstable kinetically with isomerization barriers of 7.5, 2.3, 5.3, 2.9, 2.9, and 5.5 kcal·mol^{-1}, respectively. The transition states about isomers **e12**, **e17**, **e20**, **e22**, **e27** and **e31** were not located in the current work. The ground state of **e1** can be transferred into **e11** through three direct isomerization channels. The corresponding barriers from **e11** to **e1** are 10.3, 13.8, and 28.6 kcal·mol^{-1}, respectively, suggesting that **e11** is difficult to transfer into **e1**. Interestingly, **e11** is similar to TS**e1/e11(I)**

Table 1 The relative energies (kcal·mol^{-1}) of lower-energy isomers for B_nPt (n=1-6) at the different theoretical levels

Clusters	Isomers	ΔE^{I}	ΔE^{II}	Clusters	Isomers	ΔE^{I}	ΔE^{II}	Clusters	Isomers	ΔE^{I}	ΔE^{II}
BPt	a1	0	0		d26	87.3	96.0		e30	76.6	72.4
	a2	65.7	72.5		d27	120.4	97.7		e31	70.5	75.1
B_2Pt	b1	0	0		d28	101.7	98.1		e32	78.4	78.8
	b2	28.7	36.2		d29	94.2	100.0		e33	67.0	79.7
	b3	27.2	37.5		d30	108.5	102.5	B_6Pt	f1	0	0
	b4	30.9	43.8		d31	115.6	102.7		f2	9.7	3.3
B_3Pt	c1	0	0		d32	128.8	105.0		f3	7.8	10.4
	c2	17.4	18.8		d33	136.4	108.4		f4	5.2	11.0
	c3	20.1	22.7		d34	133.7	108.9		f5	12.3	11.6
	c4	28.5	25.8		d35	125.5	109.1		f6	13.9	12.9
	c5	22.6	28.6		d36	115.0	112.5		f7	14.5	18.6
	c6	34.7	33.7		d37	118.9	115.4		f8	27.1	19.5
	c7	33.6	34.9		d38	131.9	118.5		f9	12.0	19.6
	c8	39.0	49.4		d39	128.6	119.5		f10	12.8	20.0
	c9	31.7	39.4		d40	138.9	133.7		f11	16.2	20.5
	c10	35.5	39.7		d41	166.9	135.5		f12	20.0	24.6
	c11	44.1	41.4	B_5Pt	e1	0	0		f13	9.0	25.3
	c12	36.9	43.1		e2	6.8	7.2		f14	27.8	28.3
	c13	56.9	57.4		e3	14.6	12.4		f15	27.4	25.6
	c14	59.8	58.6		e4	30.4	24.3		f16	22.9	29.3
B_4Pt	d1	0	0		e5	37.4	35.3		f17	36.0	30.1
	d2	24.4	29.1		e6	40.5	37.5		f18	33.0	30.6
	d3	30.0	33.9		e7	41.1	39.7		f19	27.1	31.1
	d4	37.6	37.4		e8	41.4	41.0		f20	33.7	32.0
	d5	38.0	37.4		e9	33.3	42.2		f21	29.3	32.2
	d6	41.3	40.5		e10	55.4	47.1		f22	39.8	32.6
	d7	42.5	40.7		e11	54.0	47.1		f23	33.4	32.9
	d8	42.3	41.6		e12	62.3	48.7		f24	32.4	33.1
	d9	45.2	44.8		e13	53.3	49.0		f25	27.2	34.3
	d10	58.0	48.1		e14	56.5	49.2		f26	32.6	34.8
	d11	58.3	50.0		e15	50.6	49.5		f27	45.0	35.5
	d12	58.2	60.8		e16	52.2	51.2		f28	39.5	36.0
	d13	44.6	61.0		e17	55.2	52.3		f29	38.7	36.1
	d14	70.8	61.5		e18	53.1	55.0		f30	28.1	36.8
	d15	69.0	67.9		e19	59.8	57.6		f31	53.7	37.4
	d16	65.7	69.1		e20	74.1	58.4		f32	49.1	47.1
	d17	56.1	69.2		e21	65.0	60.6		f33	60.6	48.5
	d18	80.2	70.3		e22	80.4	61.3		f34	41.0	50.1
	d19	73.4	74.0		e23	59.4	61.4		f35	56.1	50.4
	d20	68.2	74.4		e24	58.9	61.6		f36	36.7	51.0
	d21	84.1	79.0		e25	69.3	62.3		f37	51.0	53.0
	d22	83.2	81.4		e26	70.9	66.1		f38	67.2	53.0
	d23	73.7	81.6		e27	69.8	69.5		f39	63.0	54.5
	d24	96.0	82.5		e28	67.8	71.2		f40	52.6	55.1
	d25	94.2	83.6		e29	77.3	72.2				

[I] The relative energies with zero-point energy correction at the B3LYP/6-311+G(d)/LanL2DZ] level

[II] The relative energies at the CCSD(T)/6-311+G(d)/LanL2DZ]//B3LYP/6-311+G(d)/LanL2DZ] level

Table 2 Relative energies (kcal·mol^{-1}) of transition states for lower-energy isomers of B_nPt (n=2-5) at the B3LYP/6-311+G(d)/LanL2DZ] and CCSD(T)/6-311+G(d)/LanL2DZ] levels

Clusters	Species	B3LYP[a]	CCSD	Clusters	Species	B3LYP[a]	CCSD
$B_2Pt(t^b)$	TSb2/b4	85.8	93.6		TSe1/e11(III)	79.1	75.7
B_3Pt (d^b)	TSc1/c7	32.9	35.9		TSe1/e25	80.1	78.3
	TSc7/c9(I)	49.6	50.8		TSe9/e25	85.6	86.3
	TSc1/c9	42.8	53.0		TSe9/e33(I)	74.1	90.5
	TSc7/c9(II)	49.4	63.1		TSe9/e33(II)	74.9	108.3
B_3Pt (q^b)	TSc2/c3	27.5	21.1	$B_5Pt(q^b)$	TSe7/e16(I)	53.5	56.4
	TSc2/c10	36.2	42.0		TSe7/e16(II)	71.0	67.3
	TSc10/c11	45.0	42.0		TSe7/e29(I)	62.3	72.7
	TSc3/c5(I)	38.1	47.5		TSe24/e28	68.2	73.6
	TSc3/c5(II)	42.8	53.8		TSe29/e30(I)	82.4	76.0
$B_4Pt(s^b)$	TSd1/d4(I)	52.5	47.1		TSe5/e7	76.7	76.7
$B_4Pt(t^b)$	TSd1/d6	49.7	47.9		TSe5/e30	86.1	78.2
	TSd1/d5	49.5	51.6		TSe23/e28(I)	81.2	81.3
	TSd4/d6	92.7	67.0		TSe23/e28(II)	85.3	87.8
	TSd1/d4(II)	78.2	72.4		TSe7/e29(II)	96.2	88.3
	TSd1/d4(III)	81.8	78.6		TSe7/e32	91.5	94.5
	TSd33/d34	138.6	109.9		TSe29/e30(II)	100.7	95.6
$B_5Pt(d^b)$	TSd2/d3(I)	33.5	36.0		TSe23/e28(III)	123.1	114.8
	TSd3/d8	45.7	43.9				
	TSd7/d16	70.4	69.2				
	TSd3/d7	64.5	69.4				
	TSd2/d3(II)	72.1	73.7				
	TSd19/d20	77.1	85.0				
	TSd7/d15	95.4	91.0				
	TSe2/e3	16.1	14.7				
	TSe1/e2(I)	14.7	15.8				
	TSe1/e2(II)	41.4	44.0				
	TSe2/e9	39.4	47.5				
	TSe10/e11(I)	56.2	50.0				
	TSe10/e11(II)	58.4	52.4				
	TSe3/e13	58.7	54.8				
	TSe1/e11(I)	60.0	57.4				
	TSe1/e11(II)	61.6	60.9				

[a] The zero-point vibrational energy is included

[b] The letters s, t, d, and q represent singlet, triplet, doublet, and quartet states, respectively

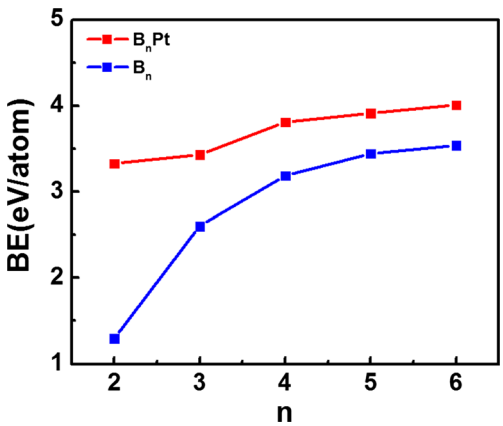

Fig. 3 The binding energy per atom versus n for the lowest-energy isomers of B_nPt and B_n clusters (*n*=2-6)

and TS**e1/e11(II)** in structure. **e11** can be transferred into TS**e1/e11(III)** by breaking of B-B bond, which may lead to higher conversion barrier than those of the other two conversion processes. The most stable **e1** of B_5Pt can be directly converted into **e2** by two different isomerization channels with the conversion barriers of 15.8 and 44.0 kcal·mol^{-1}, respectively. The conversion barriers of (**e2**→TS**e2/e3)** and (**e3**→TS**e2/e3)** are 7.5 and 2.3 kcal·mol^{-1}, respectively. It is due to the fact that the conversion process (**e2**→TS**e2/e3)** needs to break the inner B-B bond, while the conversion process (**e3**→TS**e2/e3)** needs to form two inner B-B bonds. The conversion process (**e1**→TS**e1/e25**) includes the breaking of two B-B bonds while in the conversion process (**e25**→TS**e1/e25**), **e25** and TS**e1/e25** are similar in structure, leading to that the first barrier (**e1**→TS**e1/e25,** 78.7 kcal·mol^{-1}) is larger than the second

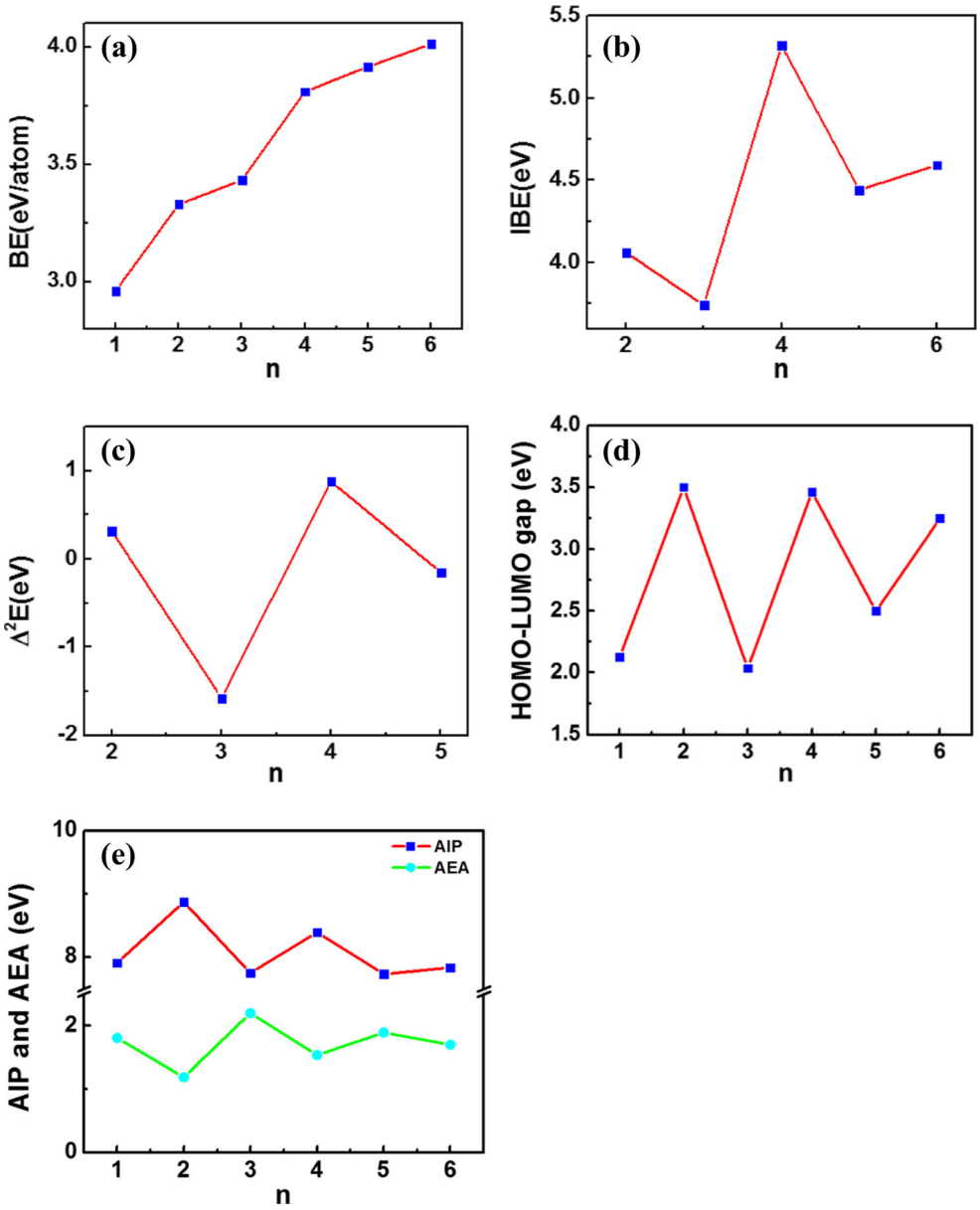

Fig. 4 The binding energy per atom (**a**), incremental binding energy (**b**), and second order difference (**c**), the HOMO-LUMO gap (**d**), the adiabatic ionization energy (AIP) and adiabatic electron affinity (AEA) (**e**) versus n for the lowest-energy isomers of B_nPt(n=1-6)

barrier (**e25**→TS**e1/e25**, 16.4 kcal·mol^{-1}). Additionally, there are two transition states for isomer pair **e10/e11.**

Table 3 Dissociation energies (kcal mol^{-1}) of the clusters B_nPt (n=1-6) at the CCSD(T)/[6-311+G(d)/LanL2DZ]//B3LYP/[6-311+G(d)/LanL2DZ] level

B_nN(n=1~6) clusters	$B_nPt \rightarrow B_{n-1}Pt+B$	$B_nPt \rightarrow B_{n-1}+BPt$
BPt ($C_{\infty v}$,$^2\sum$)	–	–
B_2Pt (C_{2v},$^1\sum_g$)	93.7	–
B_3Pt (C_{2v},$^2A_1$)	86.3	120.3
B_4Pt (C_S,$^1A'$)	122.7	122.6
B_5Pt (C_s,$^2A'$)	102.4	111.2
B_6Pt (C_S,$^3A''$)	94.9	103.0

Figure 9 demonstrates the PES of quartet B_5Pt at the CCSD/B3LYP level. Isomers **e5**, **e7**, **e23**, **e24**, and **e32** have relatively highly kinetic stability with the smallest conversion energy barriers of 41.4 (**e5**, **e5**→**e7),** 16.7 (**e7**, **e7**→**e16)**, 19.9 (**e23**, **e23**→**e28)**, 12.2 (**e24**, **e24**→**e28)**, and 15.7 (**e32**, **e32**→**e7)** kcal·mol^{-1}, respectively. The remaining isomers **e16** (**e16**→**e7**), **e28** (**e28**→**e24**), **e29** (**e29**→**e27**), and **e30** (**e30**→**e29)** are unstable kinetically with the isomerization barriers 5.2, 2.4, 0.5, and 3.6 kcal·mol^{-1}, respectively. There are not transition states about **e19** in the current calculations. The most stable isomer (**e5**) of quartet B_5Pt can be converted into **e7** and **e30** via two different conversion paths with the conversion barriers of 41.4 and 42.9 kcal·mol^{-1}, respectively. **e7** with a six-membered ring can be directly converted into isomers **e5**, **e16**, **e29**, and **e32** through different conversion

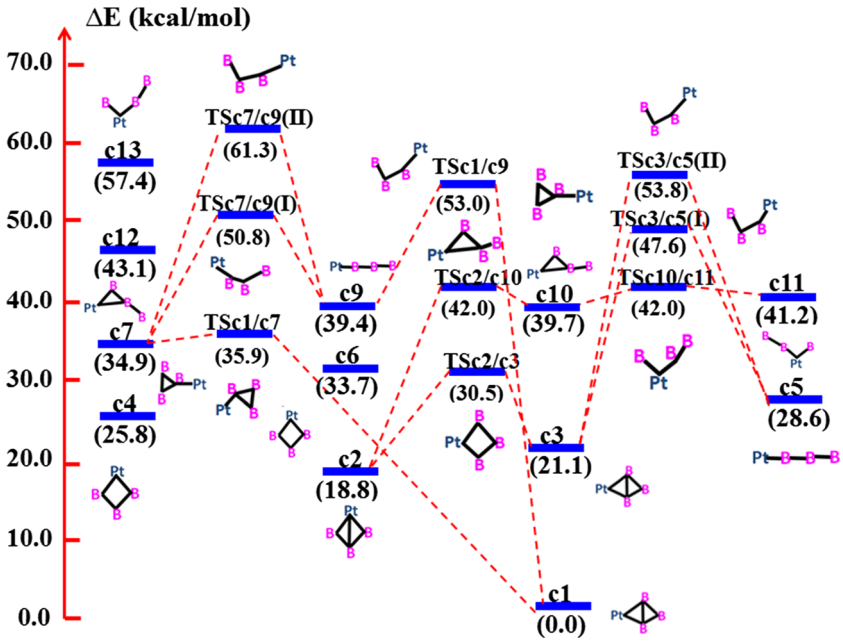

Fig. 5 Schematic potential energy surface of B_3Pt at the [CCSD(T)/6-311+G(d)/LanL2DZ]//[B3LYP/6-311+G(d)/LanL2DZ] level

paths, in which there are six transition states (TS**e5/e7**, TS**e7/e16(I)**, TS**e7/e16(II)**, TS**e7/e29(I)**, TS**e7/ e29(II)**, and TS**e7/e32**). Among these conversion processes, **e7**, TS**e7/e16(I)**, TS**e7/e16(II)**, and **e16** have a similar six-membered ring structure, but they have different inner bonds. Similarly, there are two direct conversion channels between **e29** and **e30.e7** (with cyclic structure) can be isomerized into **e32** (with a four-membered ring and one exocyclic chain), which needs to overcome the high conversion barrier of 54.8 kcal·mol^{-1} at the CCSD/B3LYP level due to the significant structural difference between them. Furthermore, there are three transition states for isomer pair **e23/e28**, and all of these conversion energy barriers are >10 kcal·mol^{-1}, revealing that the conversion **e23**→**e28** is difficult. It is easier for **e28** to convert into **e24** with barrier energy of 2.4 kcal·mol^{-1}, which can be attributed to the structural similarity of TS**e24/e28** and **e28**.

Bonding character

In order to analyze the bonding nature of B_nPt (n=1-6) clusters, the valence molecular orbitals of some planar isomers of B_nPt (n=1-6) are selected and shown in Fig. SI-2. Figure SI-2 demonstrates σ-tangential MOs (MO8 for **b1**, MO17 for **d1**, MO11 for **d33**, and MO12 for **f17**), σ-radial MOs (MO9 of

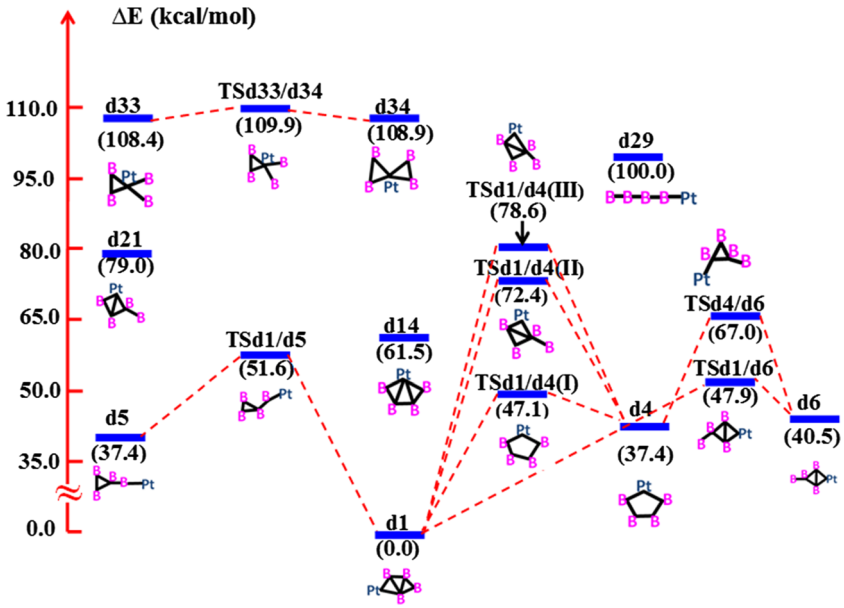

Fig. 6 Schematic potential energy surface of singlet B_4Pt at the [CCSD(T)/6-311+G(d)/LanL2DZ]//[B3LYP/6-311+G(d)/LanL2DZ] level

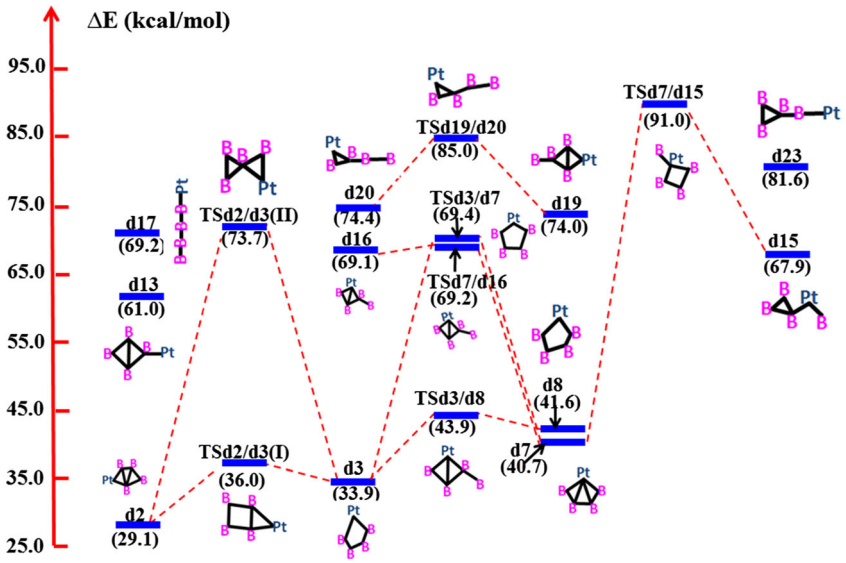

Fig. 7 Schematic potential energy surface of triplet B_4Pt at the [CCSD(T)/6-311+G(d)/LanL2DZ]//[B3LYP/6-311+G(d)/LanL2DZ] level

d14, and MO9 of **d33**), and delocalized π molecular orbitals (MO11, MO10, MO8, MO7 for **a1**, MO11, and MO9 for **b1**, MO17, MO16, MO14, and MO11 for **c1**, MO18, MO16, and MO13 for **d1**, MO18, MO16, and MO13 for **d6**, MO19, MO13, and MO12 for **d14**, MO19, MO14, and MO13 for **d33**, MO20, MO17, and MO15 for **e1,** MO21, MO20, and MO16 for **f17**, MO22, MO18, and MO17 for **f24**), which suggests that the stability of B_nPt (n=1-6) isomers is attributed to the interactions of the σ-tangential, σ-radial, and delocalized π MOs.

In order to further reveal the bonding nature of the most stable isomers of B_nPt, the electronic structure and bonding character of clusters are examined by the analyses of the electron localization function (ELF) [47] and Mayer bond order (MBO) [48]. To avoid the effects of diffuse function [49], the bond orders are calculated at the B3LYP/[6-311+G(d) /LanL2DZ] level. The ELF values within 0–1 are represented in Fig. SI-3. Moreover, the MBOs of the most stable of B_nPt (n=2-5) are shown in Fig. SI-4. It is noted that the three-center bond order of **b1** with B-Pt-B three-membered cycle is 0.132, indicating that the interactions among the three atoms are rather weak since the largest MBO value of 3c–2e is less than 0.3 [50]. Besides, as shown in Fig. SI-3, the localized electron distribution of B-Pt is longer and narrower than that

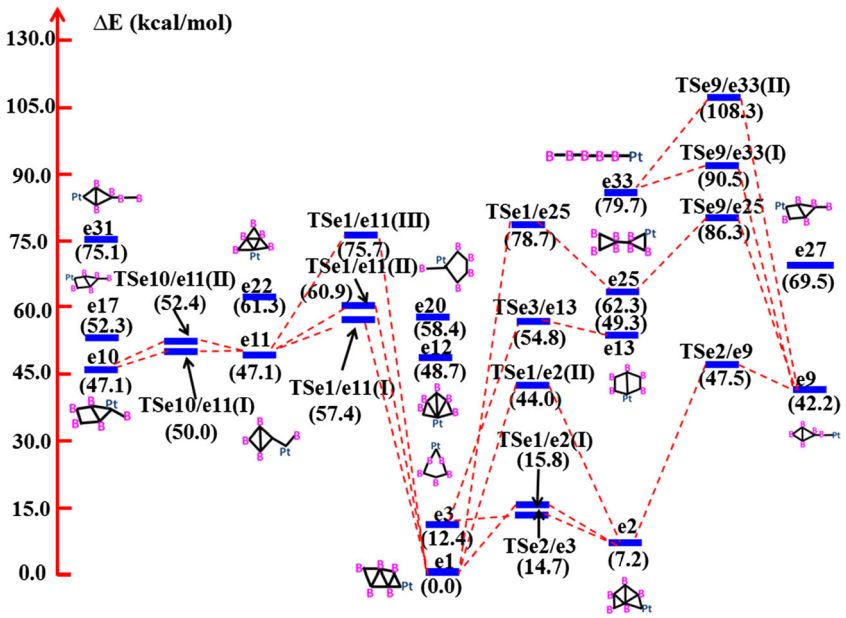

Fig. 8 Schematic potential energy surface of doublet B_5Pt at the [CCSD(T)/6-311+G(d)/LanL2DZ]//[B3LYP/6-311+G(d)/LanL2DZ] level

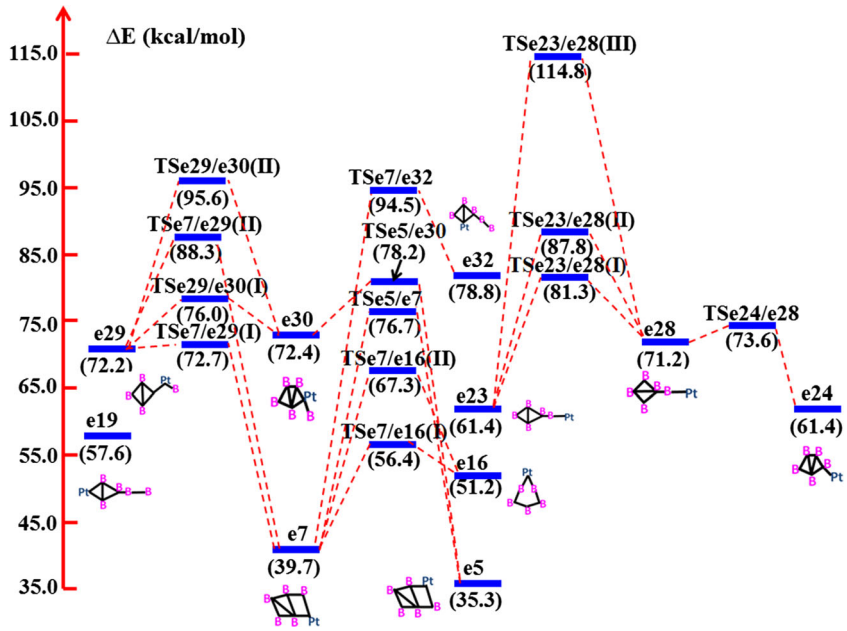

Fig. 9 Schematic potential energy surface of quartet B_5Pt at the [CCSD(T)/6-311+G(d)/LanL2DZ]//[B3LYP/6-311+G(d)/LanL2DZ] level

of B-B, which is in agreement with the MBO results (B-Pt (1.574) and B-B (1.184)). The two three-center bonds in the lowest-energy isomer of B_3Pt with C_{2v} symmetry are 0.633(B-B-B) and 0.134 (B-Pt-B), respectively, which is consistent with the results from Fig. SI-3. For **d1**, there are three three-center bonds, among which the largest MBO value of 3c–2e (B-B-B) is 0.209. The two-center MBOs in the outer cycle are 0.891-1.491, in agreement with the result of six delocalized π MOs in Fig. SI-3 and the results of Fig. SI-3, which suggests that there exists a delocalized π bond in the cycle of **d1**. Similarly, there are π bonding interactions in isomers **e1**.

As shown in Fig. SI-2, **d1** (σ-MO for MO17 and π-MOs for MO18, MO16, and MO13), **d14** (σ-MO for MO9 and π-MOs for MO19,MO13, Mo12), and **f17** (σ-MO for MO12, π-MOs for MO21, MO20, and MO16) have σ and π doubly aromatic according to Hückel (4n+2) rule. Furthermore, isomers **d6**, **d33**, **e1**, and **f24** may exhibit π-aromatic since they have six π electrons, respectively. The isomer **d33** (σ-MOs for MO11 and MO9, and π-MOs for MO19, MO14, and MO13) possesses π-aromaticity and σ-antiaromaticity. The numbers of π electrons for isomers **a1** and **b1** are 8 and 4, respectively, which may make them π-antiaromatic based on Hückel 4n rule. In order to confirm the aromaticity of those isomers, the adaptive natural density partitioning (AdNDP) method [51] is used to study electronic structure of cluster systems (Fig. 10 and Fig. SI-5). Since the AdNDP method can be applied to closed-shell systems only, we analyze and confirm the aromaticity of **d1**, **d14**, **d33**, **f17**, and **f24** in terms of AdNDP method. As shown in Fig. 10, **d1,** the

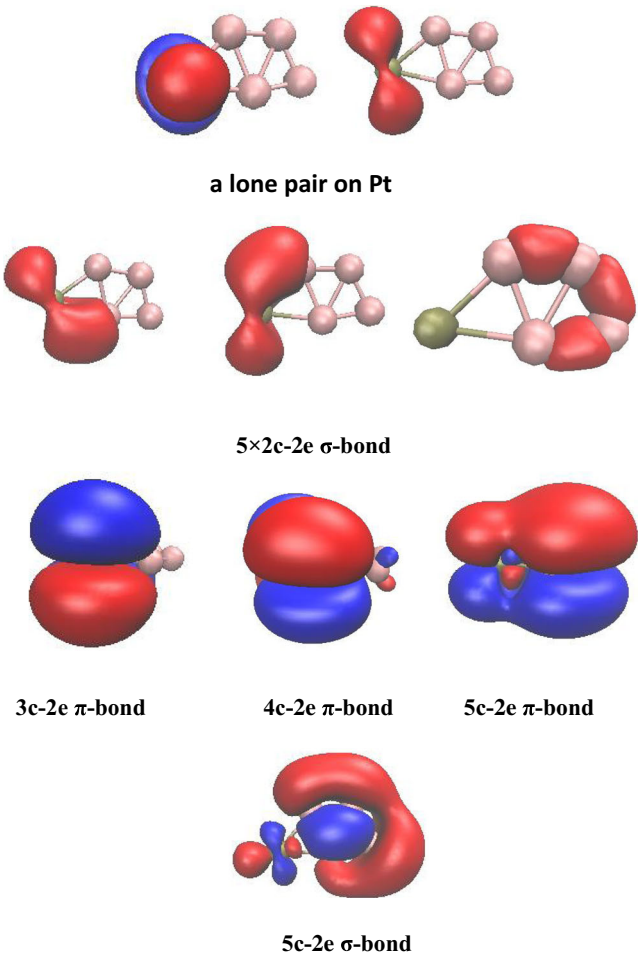

Fig. 10 The AdNDP localization results for the lower-energy isomers (**d1**) of B_4Pt

Fig. 11 ELF_{π}/ELF_{σ} plot for some isomers of B_4Pt and B_6Pt at the B3LYP/6-311+G(d) level

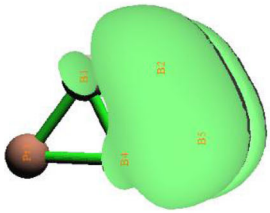

d1(ELF_{π}=0.932)

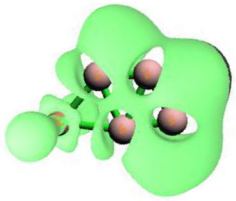

d1(ELF_{α}=0.733)

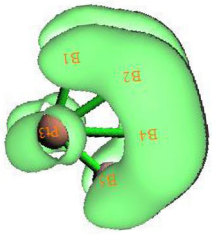

d14(ELF_{π}=0.755)

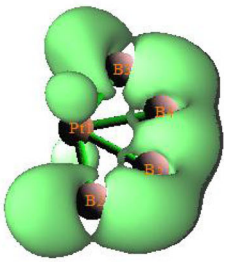

d14(ELF_{α}=0.711)

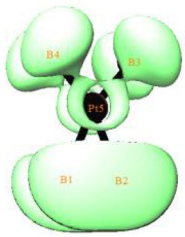

d33(ELF_{π}=0.735)

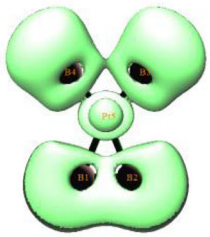

d33(ELF_{α}=0.610)

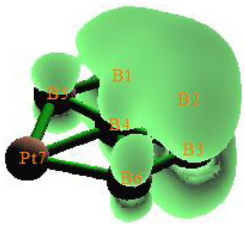

f17(ELF_{π}=0.873)

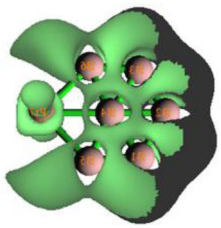

f17(ELF_{α}=0.734)

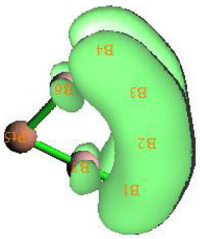

f24(ELF_{π}=0.865)

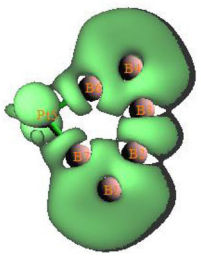

f24(ELF_{α}=0.640)

most stable structure of B_4Pt, contains two lone pairs on Pt, five 2c-2e σ-bonds, one 3c-2e π-bond, one 4c-2e π-bond, one 5c-2e π-bond, and one 5c-2e σ-bond, among which there are six delocalized π electrons and two delocalized σ electrons, satisfying with Hückel's aromatic rule of (4n+2) electrons. Figure 11 illustrates that for **d1**, ELF_π and ELF_σ values are 0.932 and 0.733, respectively, which reveals double aromaticity of **d1**. As shown in Fig. SI-5, for isomers **d14** (three 3c-2e π-bonds and one 5c-2e σ-bond) and **d33** (two 3c-2e π-bonds, one 5c-2e π-bond, two 3c-2e σ-bonds, and two 4c-2e σ-bonds), both of them have π-aromaticity and σ-antiaromaticity, which are consistent with the results of ELF_π and ELF_σ as represented in Fig. 11. Similarly, **f17** and **f24** have π-aromaticity in terms of the analyses of AdNDP and ELF as shown in Fig. SI-5 and Fig. 11. Additionally, the results of NICS and NICSzz [52] at the GIAO [53] -B3LYP/[6-311+G(d)/LanL2DZ] level also confirm their π-aromaticity. Isomers **d1**, **d14**, and **f17** exhibit σ and π doubly aromatic.

Conclusions

Many low-lying B_nPt (n=1-6) isomers are located and characterized at the CCSD/B3LYP level. B_nPt (n=2-5) clusters can be viewed as capping a Pt atom on the B-B edge of pure boron clusters. BPt has linear structure while the ground state isomer of B_6Pt adopts quasi–planar structure. Platinum doping into boron clusters can enhance the stability of pure boron clusters. The stability of B_nPt (n=1-6) clusters can be ascribed to the interactions of delocalized π, σ-radial, and σ-tangential MOs. The results obtained from the binding energies per atom, incremental binding energies, second order energy differences, and cluster decomposition analyses reveal the high stability of B_2Pt and B_4Pt. The delocalized π, σ-radial, and σ-tangential MOs play critical roles in formation of the lowest-energy isomers of B_nPt. Interestingly, isomers **d1**, **d14**, and **f17** possess σ and π doubly aromaticity, which is certified by valence molecular orbital and other (ELF, AdNDP, and NICS) analyses. The isomers **b2**, **c1**, **c2**, **d1**, and **e1** are stable both thermodynamically and kinetically, revealing that they are detectable in experiment. Importantly, the results from thermodynamic/kinetic stability and bonding character suggest that B_2Pt B_4Pt may be magic clusters. The above results can motivate future experiments about B_nPt clusters.

Acknowledgements This work is supported by grants from the National Science Foundation of China (Nos. 21276122, 21136001, and 20876073) and State Key Laboratory of Materials-Oriented Chemical Engineering, College of Chemistry and Chemical Engineering, Nanjing University of Technology of China (No. ZK201212).

References

1. Zhang GL, Yuan HK, Chen HA, Kuang L, Tian CL, Wang JZ (2014) Emergence of antiferromagnetic ordering in Tb_n (n=2–33) clusters. J Phys Chem A 118:1936–1947
2. Goto E, Begum RA, Ueno C, Hosokawa A, Yamamoto C, Nakamae K, Kure B, Nakajima T, Kajiwara T, Tanase T (2014) Electron-deficient $Pt_2M_2Pt_2$ hexanuclear metal strings (M=Pt, Pd) supported by triphosphine ligands. Organometallics 33:1893–1904
3. Paranthaman S, Hong K, Kim J, Kim DE, Kim TK (2013) Density functional theory assessment of molecular structures and energies of neutral and anionic Al_n (n=2–10) clusters. J Phys Chem A 117:9293–9303
4. Zhu XL, Zeng XC (2003) Structures and stabilities of small silicon clusters: *ab initio* molecular-orbital calculations of Si_7-Si_{11}. J Chem Phys 118:3558–3570
5. Zhu XL, Zeng XC, Lei YA, Pan B (2004) Structures and stability of medium silicon clusters. II. *ab initio* molecular orbital calculations of Si_{12}-Si_{20}. J Chem Phys 120:8985–8995
6. Calaminici P, Köster AM, Russo N, Salahub DR (1996) A density functional study of small copper clusters: Cu_n (n≤5). J Chem Phys 105:9546–9556
7. Chang CM, Chou MY (2004) Alternative low-symmetry structure for 13-atom metal clusters. Phys Rev Lett 93:133401
8. Kato H, Yamashita K (1992) *Ab initio* MO study of neutral and cationic boron clusters. Chem Phys Lett 190:361
9. Ray AK, Havard IA, Kanal KM (1992) Structure and binding in small neutral and cationic boron clusters. Phys Rev B 45:14247–14255
10. Kawai R, Weare JH (1991) Instability of the B_{12} icosahedral cluster: rearrangement to a lower energy structure. J Chem Phys 95:1151–1158
11. Kalamse V, Gaikwad S, Chaudhari A (2010) Computational study of 5d transition metal mononitrides and monoborides using density functional method. B Mater Sci 33:233–238
12. Zhai HJ, Wang LS (2006) Gold apes hydrogen. The structure and bonding in the planar $B_7Au_2^-$ and B_7Au_2 clusters. J Phys Chem A 110:1689–1693
13. Li DZ, Li SD (2011) An *ab initio* theoretical investigation on the geometrical and electronic structures of $BAu_n^{-/0}$ (n=1-4) clusters. Int J Quantum Chem 111:4418–4424
14. Barysz M, Urban M (1997) Molecular properties of boron-coinage metal dimers: BCu, BAg, BAu. Adv Quantum Chem 28:257–272
15. Ferrão LFA, Roberto-Neto O, Machado FBC (2008) Electronic structure of CuX_y (X=B, C, N, O, F; y=0,+1,-1). Int J Quantum Chem 108:2512–2522
16. Yao JG, Wang XW, Wang YX (2008) A theoretical study on structural and electronic properties of Zr-doped B clusters: ZrB_n (n=1–12). Chem Phys 351:1–6
17. Jia JF, Ma LJ, Wang JF, Wu HS (2013) Structures and stabilities of ScB_n (n=1–12) clusters: an *ab initio* investigation. J Mol Model 19:3255–3261
18. Yang Z, Xiong SJ (2008) Structures and electronic properties of small FeB_n (n=1–10) clusters. J Chem Phys 128:184310
19. Romanescu C, Galeev TR, Li WL, Boldyrev AI, Wang LS (2011) Aromatic metal-centered monocyclic boron rings: $Co©B_8^-$ and $Ru©B_9^-$. Angew Chem Int Edit 50:9334–9337
20. Galeev TR, Romanescu C, Li WL, Wang LS, Boldyrev AI (2012) Observation of the highest coordination number in planar species: decacoordinated $Ta©B_{10}^-$ and $Nb©B_{10}^-$ Anions. Angew Chem Int Edit 51:2101–2105
21. Romanescu C, Galeev TR, Li WL, Boldyrev AI, Wang LS (2012) Transition-metal-centered monocyclic boron wheel clusters ($M©B_n$): a new class of aromatic borometallic compounds. Accounts Chem Res 46:350–358

22. Li WL, Romanescu C, Galeev TR, Piazza ZA, Boldyrev AI, Wang LS (2011) Transition-metal-centered nine-membered boron rings: M©B_9 and M©B_9^-(M=Rh, Ir). J Am Chem Soc 134:165–168
23. Romanescu C, Galeev TR, Sergeeva AP, Li WL, Wang LS, Boldyrev AI (2012) Experimental and computational evidence of octa- and nona-coordinated planariron-doped boron clusters: Fe©B_8 and Fe©B_9. J Organomet Chem 721:148–154
24. Pu Z, Ito K, Schleyer PR, Li QS (2009) Planar hepta-, octa-, nona-, and decacoordinate first row D-block metals enclosed by boron rings. Inorg Chem 48:10679–10686
25. Ge GX, Jing Q, Cao HB, Yan HX (2012) Structural, electronic, and magnetic properties of MB_n (M=Y, Zr, Nb, Mo, Tc, Ru, $n\leq 8$) clusters. J Clust Sci 23:189–202
26. Zhao YY, Zhang MY, Chen BG, Zhang J, Sun CC (2006) Theoretical study on the stability of the novel B_{32} isomers and their metal-polyboron MB_{32} cluster. J Mol Struc: Theochem 759:25–30
27. Wu GF, Wang JL, Zhang XY, Zhu LY (2009) Hydrogen storage on metal-coated B_{80} buckyballs with density functional theory. J Phys Chem C 113:7052–7057
28. Tai TB, Nhat PV, Nguyen MT, Li SG, Dixon DA (2011) Electronic structure and thermochemical properties of small neutral and cationic lithium clusters and boron-doped lithium clusters: $Li_n^{0/+}$ and $Li_nB^{0/+}$ (n=1–8). J Phys Chem A 115:7673–7686
29. Tong J, Li Y, Wu D, Li ZR, Huang XR (2009) Low ionization potentials of binuclear superalkali B_2Li_{11}. J Chem Phys 131:164307
30. Peironcely JE, Rojas-Chertó M, Fichera D, Reijmers T, Coulier L, Faulon JL, Hankemeier T (2012) OMG: open molecule generator. J Cheminformatics 4:21
31. Hay PJ, Wadt WR (1985) *Ab initio* effective core potentials for molecular calculations. Potentials for K to Au including the outermost core orbitals. J Chem Phys 82:299–310
32. Perdew JP, Burke K, Wang Y (1996) Generalized gradient approximation for the exchange-correlation hole of a many-electron system. Phys Rev B 54:16533–16539
33. Adamo C, Barone V (1999) Toward reliable density functional methods without adjustable parameters: the PBE0 model. J Chem Phys 110:6158–6170
34. Schreiner PR, Fokin AA, Pascal RA, Meijere AD (2006) Many density functional theory approaches fail to give reliable large hydrocarbon isomer energy differences. Org Lett 8: 3635–3638
35. Krishnan R, Binkley JS, Seeger R, Pople JA (2008) Self-consistent molecular orbital methods. XX. A basis set for correlated wave functions. J Chem Phys 72:650–654
36. Ruiz E, Cano J, Alvarez S, Alemany P (1999) Broken symmetry approach to calculation of exchange coupling constants for homobinuclear and heterobinuclear transition metal complexes. J Comput Chem 20:1391–1400
37. Stephens PJ, Devlin FJ, Chabalowski CF, Frisch MJ (1994) *Ab initio* calculation of vibrational absorption and circular dichroism spectra using density functional force fields. J Phys Chem 98: 11623–11627
38. Becke AD (1992) Density–functional thermochemistry. I. The effect of the exchange–only gradient correction. J Chem Phys 96:2155
39. Becke AD (1986) Density functional calculations of molecular bond energies. J Chem Phys 84:4524
40. Becke AD (1988) A multicenter numerical integration scheme for polyatomic molecules. J Chem Phys 88:2547
41. http://www.gaussian.com/g_tech/g_ur/m_citation.htm
42. Atiş M, Özdoğan C, Güvenç ZB (2007) Structure and energetic of B_n (n=2–12) clusters: electronic structure calculations. Int J Quantum Chem 107:729–744
43. Yuan HK, Chen H, Kuang AL, Wu B (2013) Spin–orbit effect and magnetic anisotropy in Pt clusters. J Magn Magn Mater 331:7–16
44. Böyükata M, Güvenç ZB (2011) Density functional study of AlB_n clusters for n=1–14. J Alloy Compd 509:4214–4234
45. Liu C, Han P, Tang M (2011) Density functional theory study of B_nC clusters. Rapid Commun Mass Sp 25:1315–1322
46. Raghavachari K, Binkley JS (1987) Structure, stability, and fragmentation of small carbon clusters. J Chem Phys 87:2191–2197
47. Lu T (2012) Multiwfn, version 2.6, Available at: http://multiwfn.codeplex.com/
48. Mayer I (1986) Bond orders and valences from *ab initio* wave functions. Int J Quantum Chem 29:477–483
49. Matito E, Poater J, Solà M (2005) Comparison of the AIM delocalization index and the mayer and fuzzy atom bond orders. J Phys Chem A 109:9904–9910
50. Kar TT, Scheiner S (1996) Three-center bond index profiles. J Mol Struc: Theochem 370:45–49
51. Zubarev DY, Boldyrev AI (2008) Developing paradigms of chemical bonding: adaptive natural density partitionin. Phys Chem Chem Phys 10:5207–5217
52. Schleyer PVR, Jiao HJ, Hommes NJR (1997) An evaluation of the aromaticity of inorganic rings: refined evidence from magnetic properties. J Am Chem Soc 119:12669–12670
53. Wolinski K, Hinton JF, Pulay P (1990) Efficient implementation of the gauge-independent atomic orbital method for NMR chemical shift calculations. J Am Chem Soc 112:8251–8260